Published in final edited form as:
*Dev Cell*. 2013 September 30; 26(6): 591–603. doi:10.1016/j.devcel.2013.08.012.

# Lamina-associated Polypeptide-1 Interacts with the Muscular Dystrophy Protein Emerin and is Essential for Skeletal Muscle Maintenance

**Ji-Yeon Shin**[1,2], **Iván Méndez-López**[1,2], **Yuexia Wang**[1,2], **Arthur P. Hays**[2], **Kurenai Tanji**[2], **Jay H. Lefkowitch**[2], **P. Christian Schulze**[1], **Howard J. Worman**[1,2,*], and **William T. Dauer**[3,4,*]

[1]Department of Medicine, College of Physicians & Surgeons, Columbia University, 630 W 168th Street, New York, NY 10032 USA

[2]Department of Pathology and Cell Biology, College of Physicians & Surgeons, Columbia University, 630 W 168th Street, New York, NY 10032 USA

[3]Department of Neurology, University of Michigan Medical School, 109 Zina Pitcher Place, Ann Arbor, MI 48109 USA

[4]Department of Cell and Developmental Biology, University of Michigan Medical School, 109 Zina Pitcher Place, Ann Arbor, MI 48109 USA

## SUMMARY

X-linked Emery-Dreifuss muscular dystrophy is caused by loss-of-function of emerin, an integral protein of the inner nuclear membrane. Yet emerin null mice are essentially normal, suggesting the existence of a critical compensating factor. We show that the lamina-associated polypeptide1 (LAP1) interacts with emerin. Conditional deletion of LAP1 from striated muscle causes muscular dystrophy and this pathology is worsened in the absence of emerin. LAP1 levels are significantly higher in mouse than human skeletal muscle and reducing LAP1 by approximately half in mice also induces muscle abnormalities in emerin null mice. Conditional deletion of LAP1 from hepatocytes yields mice that exhibit normal liver function and are indistinguishable from wild type controls. These results establish that LAP1 interacts physically and functionally with emerin and plays an essential and selective role in skeletal muscle maintenance. They also highlight how dissecting differences between mouse and human phenotypes can provide fundamental insights into disease mechanisms.

## INTRODUCTION

Mutations in genes encoding nuclear envelope proteins cause tissue-specific diseases called “laminopathies” or “nuclear envelopathies” (Dauer and Worman, 2009). For example, dominant or recessively inherited mutations in *LMNA* encoding the A-type nuclear lamins cause Emery-Dreifuss muscular dystrophy (EDMD) and phenotypically related myopathies



*Correspondence: hjw14@columbia.edu (H.J.W.), dauer@med.umich.edu (W.T.D).

SUPPLEMENTAL INFORMATION

Supplemental Information includes Supplemental Experimental Procedures and five figures and can be found with this article online at doi:X.

(Bonne et al., 1999; Fatkin et al., 1999; Muchir et al., 2000; Brodsky et al., 2000; Rafaelle di Barletta et al., 2000). EDMD is also inherited as an X-linked disorder caused by mutations in *EMD* encoding emerin (Bione et al., 1994), an integral protein of the inner nuclear membrane (INM) that interacts with A-type lamins (Manilal et al., 1996; Nagano et al., 1996; Fairley et al., 1999; Sullivan et al., 1999; Clements et al., 2000). Different mutations in *LMNA* cause diseases primarily affecting other tissue types, such as fat or peripheral nerve (Dauer and Worman, 2009).

To better understand how alterations in nuclear envelope proteins cause disease, we initiated "interactome" screens with integral proteins of the INM. We began with lamina-associated polypeptide 1 (LAP1), a type II integral protein of the INM (Senior and Gerace, 1988), because of its interactions with proteins linked to tissue-selective disease. The luminal domain of LAP1 binds to torsinA, the defective protein in the CNS specific disease DYT1 dystonia (Goodchild and Dauer, 2005), and its nucleoplasmic domain binds to lamin A (Foisner and Gerace, 1993; Maison et al., 1997; Senior and Gerace, 1988).

We find that LAP1 interacts with emerin, the X-linked EDMD protein and show that conditional deletion of LAP1 from mouse muscle causes muscular dystrophy leading to early lethality. In contrast, conditional deletion of LAP1 from liver has little or no effect at the organismal or cellular level. Although emerin null mice do not develop myopathy, emerin deficiency significantly worsens the muscular dystrophy and shortens the lifespan of mice lacking LAP1 in skeletal muscle, thus establishing a vertebrate model system in which the effects of emerin disruption on muscle pathology can be studied. The level of LAP1 in skeletal muscle of mice is approximately double that of humans and reducing it by ~50% causes a mild myopathy in emerin null mice. These data demonstrate an essential and selective role for LAP1 in striated muscle and suggest strongly that the difference in the level of skeletal LAP1 is a key factor underlying the consequences of emerin loss-of-function in humans and mice. This relationship between LAP1 and emerin is reminiscent of that between dystrophin and utrophin, which contributes to the distinct consequences of dystrophin deletion in human and mouse (Deconinck et al., 1997; Grady et al., 1997).

## RESULTS

### Emerin Interacts With LAP1

We conducted an unbiased "interactome" screen to identify LAP1-binding proteins. HEK 293 cells were stably transfected with a construct that expressed V5 epitope tagged LAP1. Immunoprecipitates of protein extracts from induced and un-induced cells obtained using anti-V5 antibodies were analyzed by mass spectroscopy. This analysis identified emerin with the highest score among candidates (Table S1).

We performed several experiments to confirm that emerin is a bona fide LAP1- interacting protein. We first repeated co-immunoprecipitations in stably transfected HEK 293 cells with the inducible construct encoding V5 epitope tagged LAP1. Endogenous emerin was co-precipitated by anti-V5 antibodies from protein extracts of induced cells but not from un-induced cells (Figure 1A). Neither MAN1 nor LAP2β that share the LEM domain with emerin were co-precipitated. A small quantity of lamin A, which binds LAP1 and emerin, was identified in immunoprecipitates (Figure 1A). To examine the emerin-LAP1 interaction at endogenous protein levels, we performed co-immunoprecipitation in un-transfected HEK 293 cells with anti-emerin antibodies. In these experiments, endogenous LAP1 was co-immunoprecipitated but LAP2β was not (Figure 1B). We further expressed the nucleoplasmic domain of emerin devoid of its transmembrane segment as a maltose-binding protein (MBP) fusion in bacteria, purified it and incubated it with a glutathione-S-transferase (GST) or a V5 fusion of full-length LAP1 purified from transfected HEK 293 cells on GST

or V5 agarose (Figure 1C). The MBP-emerin fusion protein but not MBP alone bound to the LAP1 fusions attached to the GST or V5 agarose (Figure 1C). This suggested that LAP1 interacts with emerin specifically through its nucleoplasmic domain. We tested this prediction by performing domain-mapping experiments with emerin and LAP1 or LAP1 fragments expressed in HEK 293 cells. We transfected HEK 293 cells with cDNAs encoding V5-tagged full-length LAP1, LAP1 nucleoplasmic plus transmembrane domain (first 360 amino acids) or LAP1 transmembrane plus luminal domain (amino acid 330 to amino acid 584) (Figure 1D). Immunoprecipitation with anti-V5 antibodies showed that endogenous emerin co-immunoprecipitated with full-length or nucleoplasmic plus transmembrane domain constructs but not with the transmembrane plus luminal domain construct (Figure 1E). Hence, emerin and LAP1 interact through their nucleoplasmic domains.

We next used fluorescence resonance energy transfer (FRET) acceptor photobleaching to examine the LAP1-emerin interaction in cells. With this method, increases in donor fluorescence after acceptor photobleaching measures efficiency of energy transfer (representing physical proximity) between two proteins. As a positive control, we used the GFP-lamin A/RFP-emerin pair. For negative controls, we used either GFP-LAP1/RFP or GFP/RFP-emerin pairs. Energy transfer efficiency between GFP-LAP1 and RFP-emerin was significantly greater than both negative control pairs, confirming that emerin and LAP1 interact in living cells (Figure 2A, B). Energy transfer was independent of the intensity of acceptor fluorescence (Figure 2C), indicating the FRET was not a random distribution effect but occurred as a result of specific binding between donor and acceptor molecules (Periasamy et al., 2008).

To obtain further evidence that LAP1 interacts with emerin, we examined the effects of depletion of these proteins on each other's subcellular localization. In LAP1 null fibroblasts, emerin mislocalized to distinct foci along the nuclear envelope in approximately 30% of cells examined (Figure 3A). A-type lamins co-localized with emerin in these abnormal foci, yet all other nuclear envelope proteins examined exhibited a normal distribution pattern, including lamin B1, LBR (an integral INM protein) and Nup98 (a nuclear pore complex protein) (Figure 3B). LAP1 null cells exhibited normal morphology of ER and Golgi (data not shown) and normal amounts of emerin, lamin A, lamin C and lamin B1 compared to wild type cells (Figure 3C). We also found that in emerin null fibroblasts LAP1 expression was mildly reduced but its localization in the nuclear envelope was unaltered (Figure S1A, B). These data further support a physical interaction between emerin and LAP1 and indicate that LAP1 is required for normal localization of a subpopulation of emerin/A-type lamin complexes.

We next tested whether depleting emerin or LAP1 changed the behavior of the other in cells. Emerin diffuses within the nuclear envelope membranes (Östlund et al., 1999), so we tested if its diffusional mobility was altered in the absence of LAP1 using fluorescence recovery after photobleaching (FRAP). GFP-emerin recovered more quickly in fibroblasts lacking LAP1, although the initial mobility rates as measured by $t_{1/2}$ were not significantly different between cell types (Figure 3D). Similar to the limited effects on localization observed in emerin null cells, LAP1 mobility was unchanged in the absence of emerin (data not shown). These findings show that LAP1 contributes to the immobilization of emerin in the INM, but other proteins such as A-type lamins likely play a more significant role (Sullivan et al., 1999; Östlund et al., 1999, 2006).

## Conditional Deletion of LAP1 From Muscle Causes Muscular Dystrophy

Loss of emerin causes EDMD in humans (Astejada et al., 2007; Bione et al., 1994; Manilal et al., 1996; Nagano et al., 1996). However, emerin null mice have a normal lifespan and do

not develop overt muscle pathology (Melcon et al., 2006; Ozawa et al., 2006). To begin to explore the mechanism for this striking species difference, we examined the relative levels of LAP1 and emerin in human and mouse skeletal muscle. Western blot analysis of emerin using antibodies recognizing both the mouse and human proteins revealed that mouse skeletal muscle has diminished expression compared to human (Figure 4A, B). Similar results were obtained using anti-emerin antibodies obtained from three different sources provided in Supplemental Experimental Procedures (data not shown). Conversely, LAP1 expression was significantly higher in mouse than human striated muscle (Figure 4A, B). These differences in the relative levels of LAP1 and emerin suggested that mouse skeletal muscle may be less dependent upon emerin function and potentially protected by high levels of LAP1. To test for such a functional effect of LAP1 that might parallel its interaction with emerin, we explored the effects of LAP1 depletion *in vivo* in mouse striated muscle. Because germline deletion causes perinatal lethality (Kim et al., 2010), we floxed *Tor1aip1* encoding LAP1 (Figure S2A) to conditionally delete LAP1 from striated muscle, using *Mck-Cre* transgenic mice that express Cre recombinase selectively in striated muscle. The *Mck* promoter is expressed at approximately E17 in differentiating striated muscle of mouse embryos (Brüning et al., 1998; Beedle et al., 2012). *Mck-Cre*$^{+/-}$;*Tor1aip1*$^{f/f}$ mice ("*M-CKO*" for muscle-selective conditional knockout) exhibited efficient and specific recombination at the *Tor1aip1* locus in striated muscle but not in liver or lung (Figure S2B). LAP1 was depleted selectively in protein lysates from muscle (Figure S2C, D) and undetectable in myofibers (Figure S2E).

*M-CKO* mice were born at the expected Mendelian frequency and initially indistinguishable from *Tor1aip1*$^{f/f}$ littermate controls. However, at approximately 8 weeks of age they stopped gaining weight, and over the next 4–6 weeks became noticeably smaller than littermate controls and developed an abnormal hunched posture (Figure 4C). *M-CKO* mice became significantly lighter than littermate controls by 12 weeks of age and continued to lose weight until dying prematurely (Figure 4D). This was the same for both sexes (data not shown). Body mass versus age of *Tor1aip1*$^{f/f}$ control littermates was indistinguishable from both wild type and *Mck-Cre* mice (data not shown). Male *M-CKO* mice had a median survival of approximately 150 days with 100% mortality by 211 days whereas 100% of controls survived until they were sacrificed at 275 days (Figure 4E). Similar results were obtained for female mice (data not shown). By 16 weeks of age, *M-CKO* mice had gross atrophy of multiple muscle groups compared to littermate controls (Figure 4F, G). Serum creatine phosphokinase activity was significantly elevated in *M-CKO* mice compared to age-matched controls with half having a value of 1,200 U, the assay cutoff (Figure 4H). *M-CKO* mice also had decreased grip strength compared to controls (Figure 4I). These results demonstrate that loss of LAP1 function from striated muscle causes a profound myopathy resulting in early death.

Histopathological analysis of skeletal muscle from *M-CKO* mice showed classical features of muscular dystrophy that worsened with age. Hematoxylin and eosin-stained sections of gastrocnemius muscle showed that *M-CKO* muscle appeared normal at 6 weeks but showed degenerative/regenerative fibers by 9 weeks and degenerative/regenerative fibers, central myonuclei and myonuclei arrays by 12 weeks (Figure 5A). Similar pathological features were found in tibialis anterior, soleus and diaphragm at 12 weeks of age (Figure S3A). Muscle fibers from *Mck-Cre* mice did not show these changes and there were no differences between male and female *M-CKO* mice (data not shown). By 9 weeks, there was a significant decrease in quadriceps muscle fiber area in *M-CKO* mice compared to controls (Figure 5B) and by 12 weeks approximately 40% of the myofibers had central nuclei (Figure 5C). At 16 weeks of age, quadriceps muscle from M-CKO mice had significantly increased fibrosis, which was virtually absent in controls (Figure 5D, E, F). Electron micrographs of quadriceps muscle showed changes consistent with a profound myopathy, including

disorganized myofibrils, increased sarcomere length, dispersed glycogen particles and enlarged mitochondria and nuclei (Figure 5G).

Immunofluorescence microscopic analysis of isolated myofibers from skeletal muscle of *M-CKO* revealed frequent enlarged nuclei with ruffled borders when labeled with anti-lamin A antibodies and approximately 10% exhibited punctate nuclear foci recognized by anti-emerin antibodies (Figure S3B). The abnormal localization of emerin was similar to that observed in embryonic fibroblasts of LAP1 null mice. Analysis of myofiber types showed an increase in type IIa fibers and a decrease in type IIb fibers in gastrocnemius but not soleus muscle from *M-CKO* mice compared to wild type mice at 16 weeks of age (Figure S3C, D). In Duchenne muscular dystrophy, type IIb fibers are the first to degenerate and a transformation into type IIa fibers has been postulated to occur (Webster et al., 1988; Pedemonte et al., 1999).

## Conditional Deletion of LAP1 From Liver Causes No Overt Phenotype

Tissues of endodermal origin are not typically affected in human nuclear envelope-related diseases. Specifically, patients with EDMD caused by mutations in *EMD* do not develop liver disease. To determine whether our findings in *M-CKO* mice represent a unique requirement of muscle tissue for LAP1, or reflect a non-specific role, we conditionally deleted LAP1 from hepatocytes using *Alb-Cre* transgenic mice that express *Cre* under control of an albumin promoter. *Alb-Cre*$^{+/-}$;*Tor1aip1*$^{f/f}$ mice ("*L-CKO*" for liver-selective conditional knockout) mice exhibited efficient and specific recombination at the *Tor1aip1* locus in liver but not in lung or striated muscle (Figure S4A). LAP1 was depleted selectively in protein lysates from liver (Figure S4B, C) and undetectable in hepatocytes (Figure S4D).

In marked contrast to the profound phenotype of *M-CKO* mice, *L-CKO* mice (Figure 6A) were indistinguishable from their littermate controls at all ages examined, up to 23 months. Weight gain (Figure 6B), liver size (Figure 6C) and liver to body mass ratio (Figure 6D) were normal. Moreover, hepatocyte integrity and liver function appeared unaffected, as evidenced by normal mean serum activities of aspartate and alanine aminotransferases and serum concentrations of bilirubin and albumin (Figure 6E). Histopathological examination of livers from 16 week-old *L-CKO* showed essentially normal overall tissue organization except for some slight narrowing of the sinusoidal spaces and there was no evidence of hepatitis or cirrhosis (Figure 6F). Hepatocyte nuclei did show an increase in size (Figure 6G). Lifespan of *L-CKO* mice followed for up to 690 days did not differ from controls (Figure 6H). Both male and female *L-CKO* mice were fertile up to a year of age. These data demonstrate that LAP1 is not essential in all tissues, highlighting the specificity and importance of LAP1 function in muscle.

Our data demonstrating a physical interaction between LAP1 and emerin suggest that these proteins may be functionally related and could potentially compensate for each other's absence. We therefore examined the relative levels of emerin in mouse muscle and liver and found that both tissues express similar levels (Figure 6I), eliminating the possibility that emerin "masks" an essential role for LAP1 in *M-CKO* mouse muscle. The lack of phenotype in *L-CKO* mice is even more striking considering that there is significantly more LAP1 in liver than in muscle (Figure 6I). The relevance of the mouse model to human liver is supported by the finding of similar relative amounts of LAP1 and emerin in human liver (Figure 6J). Considered together, these data demonstrate that LAP1 is not essential in all tissues, highlighting the specificity and importance of LAP1 function in muscle.

### Functional Interaction of LAP1 and Emerin Deletion in Mouse Striated Muscle

Having established that LAP1 binds to emerin and plays a specific and essential role in muscle maintenance, we next tested whether these proteins functionally interact *in vivo* in skeletal muscle, the main tissue disrupted in EDMD. We explored this question by generating mice that lacked LAP1 in striated muscle on an emerin null background (*M-CKO;Emd*$^{-/y}$ mice). The fact that emerin null mice do not develop myopathy (or any other overt phenotype) and exhibit a normal lifespan (Melcon et al., 2006; Ozawa et al., 2006) eliminated the confounding situation inherent in testing for a functional interaction between two genes when each has an independent loss-of-function phenotype. Consistent with previous reports (Melcon et al., 2006; Ozawa et al., 2006), loss of emerin alone (*Emd*$^{-/y}$ mice) did not affect lifespan (Figure 7A) or cause myopathy (data not shown). In contrast, loss of emerin function markedly and significantly decreased the lifespan and exacerbated the myopathy of *M-CKO* mice (Figure 7A - C), reducing median survival by more than half (median survival: *M-CKO;Emd*$^{+/y}$ = 150 d; *M-CKO;Emd*$^{-/y}$ = 69 d) (Figure 7A). Similarly, loss of emerin function enhanced the severity of skeletal muscle myopathic change seen in *M-CKO* mice (Figure 7B). To quantify this effect, we had the tissue independently examined by two neuromuscular pathologists unaware of the genotype (or each other's assessment). The severity scores were mostly concordant between the two pathologists: the myopathy was more severe in *M-CKO;Emd*$^{-/y}$ mice compared to male *M-CKO* mice (difference in severity score between genotypes was significant at $P = 0.0369$ for Pathologist 1 and $P = 0.0516$ for Pathologist 2). We next examined *M-CKO* heterozygous;*Emd*$^{-/y}$ mice to test if reduction of LAP1 by approximately half - to roughly the levels present in human muscle - would cause myopathic features on an emerin null background. *M-CKO* heterozygous;*Emd*$^{-/y}$ mice showed mild myopathic changes including the presence of occasional degenerative myofibers (Figure 7D). Consistent with this histopathological evidence of myopathy, *M-CKO* heterozygous;*Emd*$^{-/y}$ mice exhibit significantly elevated serum levels of creatine phosphokinase activity (Figure 7E). These mice did not exhibit overt behavioral abnormalities or reduced lifespan (data not shown). Considered together, these results suggest that emerin and LAP1 function together in skeletal muscle function and maintenance.

## DISCUSSION

Emerin loss-of-function causes EDMD in humans but progress in understanding the pathogenesis of this muscular dystrophy has been hampered by the lack of any model in which emerin loss-of-function causes overt muscle pathology. We identify LAP1 as an emerin-interacting protein and develop a model in which emerin loss-of-function causes overt skeletal muscle pathology with features of EDMD. The central myonuclei, myofiber degeneration and regeneration and elevated serum creatine phosphokinase in the mice are typical of muscular dystrophy. LAP1 thus represents an emerin-interacting protein to be functionally validated in the context of muscular dystrophy and appears to have a selective function in striated muscle. We also identify differences in the relative levels of emerin and LAP1 in human and mouse skeletal muscle that, based on additional *in vivo* findings, appear to account for the lack of muscular dystrophy phenotypes in previous emerin null mouse models. Considered together, our results demonstrate a physical and functional relationship between LAP1 and emerin in postnatal striated muscle maintenance and establish a valuable model system to dissect the pathogenesis of X-linked EDMD.

Emerin has been reported to bind to ten or more proteins (Holaska and Wilson, 2007; Wilson and Foisner, 2010). A-type lamins are the best-characterized emerin binding proteins (Fairley et al., 1999; Sullivan et al., 1999; Clements et al., 2000). Mutations in the gene encoding A-type lamins cause myopathies including autosomal EDMD (Bonne et al., 1999; Fatkin et al., 1999; Muchir et al., 2000; Brodsky et al., 2000; Rafaelle di Barletta et al.,

2000). Deletion of A-type lamins and expression of variants that cause EDMD lead to changes in emerin localization (Sullivan et al., 1999; Östlund et al., 2006; Raharjo et al., 2001). However, it remains unknown whether the muscle diseases caused by alterations in A-type lamins involve emerin dysfunction, as epistatic studies between respective mouse mutants have not been reported. Emerin interacts with the transcription factor Lmo7 and inhibits its binding to promoters of *MyoD* and *Pax3*, which are involved in myogenic differentiation (Dedeic et al., 2011). Deletion of *Lmo7* and a neighboring gene *Uchl3* lead to skeletal muscle degeneration and multiple other defects in mice, but a potential role for emerin has not been elucidated (Semenova et al., 2003). None of the other reported emerin-binding proteins has been related to muscle pathology.

We identify a physical relationship between emerin and LAP1 and, in contrast to previously identified emerin interacting proteins, present *in vivo* studies demonstrating clearly that loss of LAP1 causes myopathy sufficiently severe to cause early lethality. Furthermore, we demonstrate that LAP1 loss-of-function does not impair hepatocyte function, indicating a specific role for LAP1 in striated muscle. The dramatic difference between LAP1 loss-of-function in striated muscle and hepatocytes is consistent with several observations indicating a particular susceptibility of striated muscle to nuclear envelope dysfunction (Roux and Burke, 2007; Dauer and Worman, 2009).

The vast majority of EDMD-causing *EMD* mutations abolish emerin expression (Bione et al., 1994; Manilal et al, 1996; Nagano et al., 1996; Yates and Wehnert, 1999). Subjects with these mutations show no apparent abnormalities at birth. Joint contractures typically occur in the first decade of life, progressive muscle weakness and wasting in the second decade and cardiomyopathy in the second decade or later (Emery and Dreifuss, 1966). This classical clinical phenotype, as well as variations that can occur with *EMD* mutations (Astejada et al., 2007), indicates that emerin is dispensable for grossly normal striated muscle development but essential for postnatal muscle maintenance. This pattern of normal muscle development and later degeneration is recapitulated in our models. Moreover, in preliminary experiments, we find that *M-CKO* mice lacking LAP1 and both LAP1 and emerin in striated muscle have significantly decreased left ventricular fractional shortening compared to control mice at 9 to 11 weeks of age (data not shown).

Unlike humans, emerin null mice do not develop overt signs of myopathy postnatally (Melcon et al., 2006; Ozawa et al., 2006). Following toxin-induced muscle damage, regenerating skeletal muscles from these mice have abnormalities in signaling pathways that are involved in proliferation and differentiation (Melcon et al., 2006) but no differences have been reported in the susceptibility to this injury or the efficiency of tissue regeneration. Our comparative examination of emerin and LAP1 expression in mouse and human skeletal muscle suggest that mice may be protected from emerin loss because of significantly higher levels of LAP1 compared to humans.

Our finding that depletion of LAP1 from muscle of emerin-deficient mice causes a muscular dystrophy is reminiscent of the relationship between dystrophin and utrophin in Duchenne muscular dystrophy, a lethal X-linked inherited myopathy. Dystrophin loss-of-function causes Duchenne muscular dystrophy (Hoffman et al., 1987a,b) but deletion of dystrophin in *mdx* mice leads to a milder progressive myopathy than in humans. However, depletion of the functionally related protein utrophin from *mdx* mice causes a severe phenotype similar to Duchene muscular dystrophy (Deconinck et al., 1997; Grady et al., 1997), even though utrophin deletion itself has little effect. Similarly, LAP1, a nuclear envelope protein that binds to emerin, appears to compensate for the loss of emerin in striated muscle in mice. As the utrophin-dystrophin-deficient mouse has served as a small animal model for Duchenne muscular dystrophy, emerin-deficient mice with reduced or absent LAP1 in striated muscle

may serve as models to study X-linked EDMD. These examples highlight the importance of not focusing exclusively on the "disease" protein when considering the reasons for the presence or lack of phenotype in an animal model and demonstrate how systematically probing species differences can provide insight into disease pathogenesis. Finally, our results indicate that LAP1 loss-of-function should be considered in human subjects with EDMD phenotypes in which the genetic cause has not been established, including those that may have coexistent dystonia, as LAP1 also binds to torsinA (Goodchild and Dauer, 2005).

## EXPERIMENTAL PROCEDURES

Complete methods can be found in Supplemental Experimental Procedures.

### Cell Culture, Cell Lines and Plasmids

Fibroblasts were isolated from E14-E16 mouse embryos and cultured in Dulbecco's Modified Eagle Medium supplemented with 10% fetal bovine serum and 1% penicillin/streptomycin (all from Life Technologies) at 37 °C and 5% $CO_2$. HEK 293 cells were from American Tissue Culture Collection and maintained under the same conditions. To generate a LAP1 expressing stable cell line, a previously described full-length LAP1 cDNA fused to an N-terminal V5 epitope tag (Kim el al. 2010) was subcloned into pcDNA5FRT/TO using the Hind III and Xho I restriction sites. This plasmid was subsequently used for generation of a stable, inducible cell line expressing V5-tagged full-length LAP1 by transfection into Flp-In T-Rex-293 cells according to the manufacturer's instruction (Life Technologies). Plasmids used for co-immunoprecipitation experiments, pull-downs, FRET and FRAP are described in Supplemental Experimental Procedures.

### Identification of LAP1 Interacting Proteins by Mass Spectrometry

A doxycycline inducible V5-tagged LAP1-expressing stable cell line was used. Proteins were extracted from crude nuclear fractions obtained from un-induced cells and cells induced with doxycycline and immunoprecipitation with anti-V5 antibodies (Life Technologies) was performed in buffer containing 1% Nonidet P-40 as described in Supplemental Experimental Procedures. After immunoprecipitation, bound proteins were eluted and separated by SDS-PAGE. Bands visualized by silver staining and those in extracts of induced but not un-induced cells were cut out and subjected to in-gel trypsin digestion followed by liquid chromatography-mass spectroscopy/mass spectroscopy (Proteomics Resource Center, Rockefeller University).

### Co-immunoprecipitation and Immunoblotting

Co-immunoprecipitation was performed on protein extracts in buffer containing 1% Nonidet P-40 using anti-V5 affinity agarose (Life Technologies), anti-emerin (Vector Labs, 4G5) or anti-immunoglobulin $G_1$ (Santa Cruz) antibodies. Co-immunoprecipitated proteins were separated by SDS-PAGE and identified by immunoblotting with anti-V5 (Life Technologies), anti-emerin, anti-MAN1 (Pan et al., 2005), anti-LAP2β (Sigma) or anti-lamin A (Santa Cruz, H-102) antibodies. Details provided in Supplemental Experimental Procedures.

### Fusion Protein Purification and Pull-down Assay

MBP-emerin fusion protein was purified using pMAL Protein Fusion and Purification System according to the manufacturer's instruction (New England Biolabs). Briefly, thefirst 222 amino acids of emerin fused to MBP was expressed in *E. coli* strain C2523 and induced at 32 °C for 3 hrs with 0.3 mM isopropylthiogalactoside, purified using amylose resin and then eluted with 20 mM Tris-HCl pH 7.4, 200 mM NaCl, 1 mM EDTA, 10 mM maltose

containing protease inhibitors. Eluted proteins were dialyzed in 25 mM Tris-HCl pH 7.4, 200 mM NaCl, 1 mM EDTA. Plasmids encoding V5-tagged or GST-tagged full-length LAP1 were transfected into HEK 293 cells and expression of fusion proteins was detected by immunoblotting with anti-V5 and anti-GST (Sigma) antibodies. Additional details provided in Supplemental Experimental Procedures.

### FRAP and FRET

FRAP was performed as described (Östlund et al., 2009) and details provided in Supplemental Experimental Procedures. FRET was measured by acceptor photobleaching using the FRET Wizard in the Leica Advanced Fluorescence Application Suite (Huranova et al. 2009). HEK 293 cells were co-transfected with plasmids expressing the following protein pairs: EGFP-LAP1/RFP-emerin, EGFP-lamin A/RFP-emerin, EGFP-LAP1/RFP and EGFP/RFP-emerin. After 24 hr, cells were fixed with 4% paraformaldehyde and then washed with PBS. Cells with comparable levels of RFP and GFP fluorescence intensity were selected for analysis. Images were acquired with a 60x NA 1.40 oil objective on a laser-scanning confocal microscope (TCS SP5, Leica). Regions of the nuclear envelope were photobleached with repeated exposure to a 543 nm laser (100% power level). FRET efficiency (E) was calculated as the percentage increase in donor fluorescence after acceptor photobleaching using the formula $E = 100\times(1\text{-GFPpre/GFPpost})$.

### Human subjects

Biopsies of lateral quadriceps muscle were obtained from healthy control subjects using the Bergstrom technique under local anesthesia. Subjects were recruited from clinics at Columbia University Medical Center and written informed consent obtained. Human liver samples were obtained from the Herbert Irving Comprehensive Cancer Center tissue bank at Columbia University. The Columbia University Medical Center Institutional Review Board approved the protocols.

### Mouse Breeding and Genotyping

The Institutional Animal Care and Use Committee of Columbia University Medical Center approved all protocols. Mice were kept at room temperature and fed normal chow. *Tor1aip1* knockout mice were described previously (Kim et al., 2010). Emerin knockout mice (Melcon et al., 2006) were kindly provided by Dr. Colin L. Stewart and maintained on a C57BL/6 background. Mice carrying floxed alleles of *Tor1aip1* (*Tor1aip1*$^{f/f}$) were generated by insertion of a targeting vector into the last exon (See Supplemental Figure 1). They were crossed to *Mck-Cre* transgenic mice (Brüning et al, 1998) or *Alb-Cre* mice (Postic et al., 1999) obtained from Jackson Laboratory (see Supplemental Experimental Procedures for details). The mouse line carrying floxed alleles was crossed six times onto the C57BL/6 background. Mice were monitored and body mass measured weekly after weaning. Genotypes were determined by PCR analysis using primers described in Supplemental Experimental Procedures.

### Serum Biochemistry

Serum biochemical analysis was performed on an AutoAnalyzer in the Comparative Pathology Laboratory at Columbia University Medical Center as described (Muchir et al., 2012). Serum was separated from blood and stored at −80°C until analyzed.

### Grip Strength Analysis

Grip strength was assessed using a published protocol (Spurney et al., 2009) and a Chatillon DFIS-2 digital force gauge pull meter with angled mesh assembly. Each mouse was placed in front of the instrument and allowed to grasp the pull bar with both forelimbs and

hindlimbs and then pulled backward by its tail until its grip was broken. Force applied to the bar the moment the grasp was released was automatically recorded. Untrained mice were tested three times in succession without rest.

### Immunohistochemistry and Histopathological Analyses

Mouse skeletal muscle and liver were dissected and either fixed in 4% formaldehyde for 48 hrs or rapidly frozen in liquid nitrogen-cooled isopentane for sectioning on a cryostat. Cryosections were cut at 5-μm thickness and processed for immunohistochemistry using on M.O.M kit (Vector Labs). Primary antibodies were anti-LAP1, anti-emerin, anti-lamin A and anti-lamin B1 antibodies. Alexa Fluor 488 conjugated secondary antibody (Molecular Probes) was used to visualize the primary antibody labeling. Coverslips were mounted with Prolong Gold Anti-fade with 4′,6-diamidino-2-phenylindole (DAPI, Life Technologies) and images acquired with Zeiss Axiovert 200 M microscope attached to a Zeiss LSM 510 confocal laser scanning system (Carl Zeiss). Additional information is provided in Supplemental Experimental Procedures.

To score histopathology, two independent neuromuscular pathologists (A.P.H. and K.T.) performed blinded examination of hematoxylin and eosin-stained stained sections from quadriceps of 9–10 week-old mice. Myofibers with central nuclei and necrosis/degeneration were scored from examining 4 different sections per animal from 7 mice per group. Stained sections were graded from 0 to 3 according to severity: 0 = no pathology, 1 = focal or regional myofiber degeneration/necrosis, 2 = obvious myofiber degeneration/necrosis but less than 50% of total muscle area involved or 3 = obvious myopathy and higher than 50% of total muscle area involved.

### Electron Microscopy

Electron microscopy was performed as described previously (Kim el al., 2010). Briefly, 12-week old control and *M-CKO* mice were transcardially perfused with 4% paraformaldehyde/3% glutaraldehyde in 0.1 M sodium phosphate buffer (pH 7.4). Quadriceps were dissected and postfixed with 1% osmium tetroxide in 0.1 M cacodylate buffer (pH 7.4), incubated with uranyl acetate and dehydrated with ethanol. Tissues were subsequently rinsed with propylene oxide and embedded. Sections 60 nm thick were counterstained with uranyl acetate and lead citrate and examined on a JEM-1200EX electron microscope (JEOL).

### Statistics

Statistical significance was determined by Student's *t* test or 1-way ANOVA. GraphPad PRISM software (Version 4.0b) was used for the statistical analyses and $P < 0.05$ was considered a statistically significant difference. Survival curves were compared using the log-rank test.

## Supplementary Material

Refer to Web version on PubMed Central for supplementary material.

## Acknowledgments

We thank Colin L. Stewart for emerin null mice, Connie E. Kim generating LAP1 plasmids, Kunxin Luo and Harald Herrmann for antibodies, Jens Fielitz for ATPase staining protocols, Cecilia Östlund and James J. Dowling for comments on the manuscript and Henrik Molina for mass spectrometry data analysis. J.S. is a recipient of a Development Grant from the Muscular Dystrophy Association (MDA #171880). This work was supported by NIH/NIAMS Grant AR048997 to H.J.W. and a University of Michigan Neuroscience Scholar Award to W.T.D.

## References


Astejada MN, Goto K, Nagano A, Ura S, Noguchi S, Nonaka I, Nishino I, Hayashi YK. Emerinopathy and laminopathy clinical, pathological and molecular features of muscular dystrophy with nuclear envelopathy in Japan. Acta Myol. 2007; 26:159–164. [PubMed: 18646565]

Beedle AM, Turner AJ, Saito Y, Lueck JD, Foltz SJ, Fortunato MJ, Nienaber PM, Campbell KP. Mouse fukutin deletion impairs dystroglycan processing and recapitulates muscular dystrophy. J Clin Invest. 2012; 122:3330–3342. [PubMed: 22922256]

Bione S, Maestrini E, Rivella S, Mancini M, Regis S, Romeo G, Toniolo D. Identification of a novel X-linked gene responsible for Emery-Dreifuss muscular dystrophy. Nat Genet. 1994; 8:323–327. [PubMed: 7894480]

Bonne G, Di Barletta MR, Varnous S, Bécane HM, Hammouda EH, Merlini L, Muntoni F, Greenberg CR, Gary F, Urtizberea JA, et al. Mutations in the gene encoding lamin A/C cause autosomal dominant Emery-Dreifuss muscular dystrophy. Nat Genet. 1999; 21:285–288. [PubMed: 10080180]

Brodsky GL, Muntoni F, Miocic S, Sinagra G, Sewry C, Mestroni L. Lamin A/C gene mutation associated with dilated cardiomyopathy with variable skeletal muscle involvement. Circulation. 2000; 101:473–476. [PubMed: 10662742]

Brüning JC, Michael MD, Winnay JN, Hayashi T, Hörsch D, Accili D, Goodyear LJ, Kahn CR. Mol. Cell. 1998; 2:559–569.

Cance WG, Chaudhary N, Worman HJ, Blobel G, Cordon-Cardo C. Expression of the nuclear lamins in normal and neoplastic human tissues. J Exp Clin Cancer Res. 1992; 11:233–246.

Clements L, Manilal S, Love DR, Morris GE. Direct interaction between emerin and lamin A. Biochem Biophys Res Commun. 2000; 267:709–714. [PubMed: 10673356]

Dauer WT, Worman HJ. The nuclear envelope as a signaling node in development and disease. Dev Cell. 2009; 17:626–638. [PubMed: 19922868]

Deconinck AE, Rafael JA, Skinner JA, Brown SC, Potter AC, Metzinger L, Watt DJ, Dickson JG, Tinsley JM, Davies KE. Utrophin-dystrophin-deficient mice as a model for Duchenne muscular dystrophy. Cell. 1997; 90:717–727. [PubMed: 9288751]

Dedeic Z, Cetera M, Cohen TV, Holaska JM. Emerin inhibits Lmo7 binding to the Pax3 and MyoD promoters and expression of myoblast proliferation genes. J Cell Sci. 2011; 124:1691–1702. [PubMed: 21525034]

Dreger CK, Konig AR, Spring H, Lichter P, Herrmann H. Investigation of nuclear architecture with a domain-presenting expression system. J Struct Biol. 2002; 140:100–115. [PubMed: 12490158]

Emery AE, Dreifuss FE. Unusual type of benign x-linked muscular dystrophy. J Neurol Neurosurg Psychiatry. 1966; 29:338–342. [PubMed: 5969090]

Fairley EA, Kendrick-Jones J, Ellis JA. The Emery-Dreifuss muscular dystrophy phenotype arises from aberrant targeting and binding of emerin at the inner nuclear membrane. J Cell Sci. 1999; 112:2571–2582. [PubMed: 10393813]

Fatkin D, MacRae C, Sasaki T, Wolff MR, Porcu M, Frenneaux M, Atherton J, Vidaillet HJ Jr, Spudich S, De Girolami U, et al. Missense mutations in the rod domain of the lamin A/C gene as causes of dilated cardiomyopathy and conduction-system disease. N Engl J Med. 1999; 341:1715–1724. [PubMed: 10580070]

Foisner R, Gerace L. Integral membrane proteins of the nuclear envelope interact with lamins and chromosomes, and binding is modulated by mitotic phosphorylation. Cell. 1993; 73:1267–1279. [PubMed: 8324822]

Goodchild RE, Dauer WT. The AAA+ protein torsinA interacts with a conserved domain present in LAP1 and a novel ER protein. J Cell Biol. 2005; 168:855–862. [PubMed: 15767459]

Goodchild RE, Kim CE, Dauer WT. Loss of the dystonia-associated protein torsinA selectively disrupts the neuronal nuclear envelope. Neuron. 2005; 48:923–932. [PubMed: 16364897]

Grady RM, Teng H, Nichol MC, Cunningham JC, Wilkinson RS, Sanes JR. Skeletal and cardiac myopathies in mice lacking utrophin and dystrophin: a model for Duchenne muscular dystrophy. Cell. 1997; 90:729–738. [PubMed: 9288752]

Hoffman EP, Brown RH Jr, Kunkel LM. Dystrophin: the protein product of the Duchenne muscular dystrophy locus. Cell. 1987a; 51:919–928. [PubMed: 3319190]

Hoffman EP, Knudson CM, Campbell KP, Kunkel LM. Subcellular fractionation of dystrophin to the triads of skeletal muscle. Nature. 1987b; 330:754–758. [PubMed: 2447503]

Holaska JM, Wilson KL. An emerin “proteome”: purification of distinct emerin-containing complexes from HeLa cells suggests molecular basis for diverse roles including gene regulation, mRNA splicing, signaling, mechanosensing, and nuclear architecture. Biochemistry. 2007; 46:8897–8908. [PubMed: 17620012]

Huranova M, Jablonski JA, Benda A, Hof M, Stanek D, Caputi M. In vivo detection of RNA-binding protein interactions with cognate RNA sequences by fluorescence resonance energy transfer. RNA. 2009; 15:2063–2071. [PubMed: 19767419]

Kim CE, Perez A, Perkins G, Ellisman MH, Dauer WT. A molecular mechanism underlying the neural-specific defect in torsinA mutant mice. Proc Natl Acad Sci USA. 2010; 107:9861–9866. [PubMed: 20457914]

Maison C, Pyrpasopoulou A, Theodoropoulos PA, Georgatos SD. The inner nuclear membrane protein LAP1 forms a native complex with B-type lamins and partitions with spindle-associated mitotic vesicles. EMBO J. 1997; 16:4839–4850. [PubMed: 9305626]

Manilal S, Nguyen TM, Sewry CA, Morris GE. The Emery-Dreifuss muscular dystrophy protein, emerin, is a nuclear membrane protein. Hum Mol Genet. 1996; 5:801–808. [PubMed: 8776595]

Melcon G, Kozlov S, Cutler DA, Sullivan T, Hernandez L, Zhao P, Mitchell S, Nader G, Bakay M, Rottman JN, et al. Loss of emerin at the nuclear envelope disrupts the Rb1/E2F and MyoD pathways during muscle regeneration. Hum Mol Genet. 2006; 15:637–651. [PubMed: 16403804]

Muchir A, Bonne G, van der Kooi AJ, van Meegen M, Baas F, Bolhuis PA, de Visser M, Schwartz K. Identification of mutations in the gene encoding lamins A/C in autosomal dominant limb girdle muscular dystrophy with atrioventricular conduction disturbances (LGMD1B). Hum Mol Genet. 2000; 9:1453–1459. [PubMed: 10814726]

Muchir A, Reilly SA, Wu W, Iwata S, Homma S, Bonne G, Worman HJ. Treatment with selumetinib preserves cardiac function and improves survival in cardiomyopathy caused by mutation in the lamin A/C gene. Cardiovasc Res. 2012; 93:311–319. [PubMed: 22068161]

Nagano A, Koga R, Ogawa M, Kurano Y, Kawada J, Okada R, Hayashi YK, Tsukahara T, Arahata K. Emerin deficiency at the nuclear membrane in patients with Emery-Dreifuss muscular dystrophy. Nat Genet. 1996; 12:254–259. [PubMed: 8589715]

Östlund C, Ellenberg J, Hallberg E, Lippincott-Schwartz J, Worman HJ. Intracellular trafficking of emerin, the Emery-Dreifuss muscular dystrophy protein. J Cell Sci. 1999; 112:1709–1719. [PubMed: 10318763]

Östlund C, Folker ES, Choi JC, Gomes ER, Gundersen GG, Worman HJ. Dynamics and molecular interactions of linker of nucleoskeleton and cytoskeleton (LINC) complex proteins. J Cell Sci. 2009; 122:4099–4108. [PubMed: 19843581]

Östlund C, Sullivan T, Stewart CL, Worman HJ. Dependence of diffusional mobility of integral inner nuclear membrane proteins on A-type lamins. Biochemistry. 2006; 45:1374–1382. [PubMed: 16445279]

Ozawa R, Hayashi YK, Ogawa M, Kurokawa R, Matsumoto H, Noguchi S, Nonaka I, Nishino I. Emerin-lacking mice show minimal motor and cardiac dysfunctions with nuclear-associated vacuoles. Am J Pathol. 2006; 168:907–197. [PubMed: 16507906]

Pan D, Estevez-Salmeron LD, Stroschein SL, Zhu X, He J, Zhou S, Luo K. The integral inner nuclear membrane protein MAN1 physically interacts with the R-Smad proteins to repress signaling by the transforming growth factor-β superfamily of cytokines. J Biol Chem. 2005; 280:15992–16001. [PubMed: 15647271]

Pedemonte M, Sandri C, Schiaffino S, Minetti C. Early decrease of IIx myosin heavy chain transcripts in Duchenne muscular dystrophy. Biochem Biophys Res Commun. 1999; 255:466–469. [PubMed: 10049732]

Periasamy A, Wallrabe H, Chen Y, Barroso M. Chapter 22: Quantitation of protein-protein interactions: confocal FRET microscopy. Methods Cell Biol. 1998; 89:569–598. [PubMed: 19118691]

Postic C, Shiota M, Niswender KD, Jetton TL, Chen Y, Moates JM, Shelton KD, Lindner J, Cherrington AD, Magnuson MA. Dual roles for glucokinase in glucose homeostasis as determined

by liver and pancreatic beta cell-specific gene knock-outs using Cre recombinase. J Biol Chem. 1999; 274:305–315. [PubMed: 9867845]

Raffaele Di Barletta M, Ricci E, Galluzzi G, Tonali P, Mora M, Morandi L, Romorini A, Voit T, Orstavik KH, Merlini L, et al. Different mutations in the LMNA gene cause autosomal dominant and autosomal recessive Emery-Dreifuss muscular dystrophy. Am J Hum Genet. 2000; 66:1407–1412. [PubMed: 10739764]

Raharjo WH, Enarson P, Sullivan T, Stewart CL, Burke B. Nuclear envelope defects associated with LMNA mutations cause dilated cardiomyopathy and Emery-Dreifuss muscular dystrophy. J Cell Sci. 2001; 114:4447–4457. [PubMed: 11792810]

Roux KJ, Burke B. Nuclear envelope defects in muscular dystrophy. Biochim Biophys Acta. 2007; 1772:118–127. [PubMed: 16904876]

Semenova E, Wang X, Jablonski MM, Levorse J, Tilghman SM. An engineered 800 kilobase deletion of Uchl3 and Lmo7 on mouse chromosome 14 causes defects in viability, postnatal growth and degeneration of muscle and retina. Hum Mol Genet. 2003; 12:1301–1312. [PubMed: 12761045]

Senior A, Gerace L. Integral membrane proteins specific to the inner nuclear membrane and associated with the nuclear lamina. J Cell Biol. 1988; 107:2029–3036. [PubMed: 3058715]

Spurney CF, Gordish-Dressman H, Guerron AD, Sali A, Pandey GS, Rawat R, Van Der Meulen JH, Cha HJ, Pistilli EE, Partridge TA, et al. Preclinical drug trials in the mdx mouse: assessment of reliable and sensitive outcome measures. Muscle Nerve. 2009; 39:591–602. [PubMed: 19260102]

Sullivan T, Escalante-Alcalde D, Bhatt H, Anver M, Bhat N, Nagashima K, Stewart CL, Burke B. Loss of A-type lamin expression compromises nuclear envelope integrity leading to muscular dystrophy. J Cell Biol. 1999; 147:913–920. [PubMed: 10579712]

Webster C, Silberstein L, Hays AP, Blau HM. Fast muscle fibers are preferentially affected in Duchenne muscular dystrophy. Cell. 1988; 52:503–513. [PubMed: 3342447]

Wilson KL, Foisner R. Lamin-binding proteins. Cold Spring Harb Perspect Biol. 2010; 2:a000554. [PubMed: 20452940]

Yates JR, Wehnert M. The Emery-Dreifuss Muscular Dystrophy Mutation Database. Neuromuscul Disord. 1999; 9:199. [PubMed: 10382916]

## Highlights

- Physical interaction between inner nuclear membrane proteins LAP1 and emerin
- Functional interaction between LAP1 and emerin in striated muscle maintenance
- A mouse model to study emerin deficiency in Emery-Dreifuss muscular dystrophy

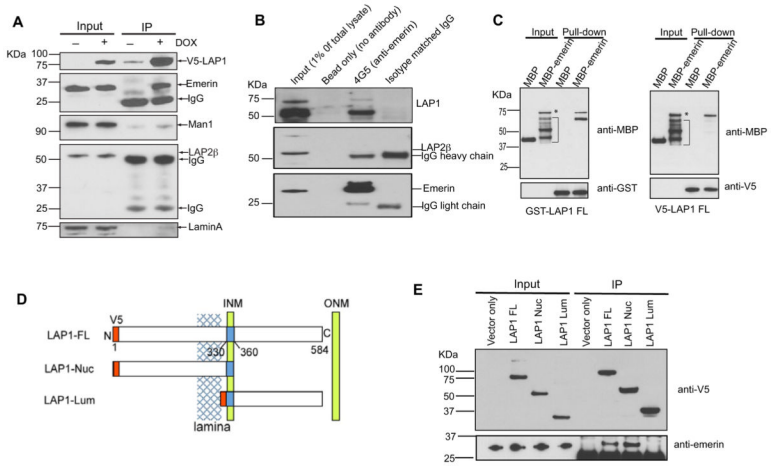


**Figure 1. LAP1 and Emerin Co-immunoprecipitate from Cell Extracts**

(A) Endogenous emerin was co-immunopreciptated with overexpressed V5-tagged LAP1 in HEK 293 cells. Protein extracts from un-induced (− DOX) or induced (+ DOX) cells were collected and immunoprecipitated (IP) with anti-V5 antibodies. Protein inputs (1% of total lysate) and precipitated products were separated by SDS-PAGE, transferred to nitrocellulose and probed with antibodies against V5, emerin, Man1, LAP2β and lamin A, the migrations of which are indicated. Migrations of molecular mass standards in KDa are indicated at the left of the blots.

(B) Protein extracts from HEK 293 cells were incubated with anti-emerin (4G5), isotype matched anti-immunoglobulin G (IgG) and agarose beads with no antibody for co-immunoprecipitation. LAP1 co-immunoprecipitated with emerin but LAP2β did not as indicated in the immunoblot. Double band of emerin may be due to differential phosphorylation. Bands corresponding to IgG heavy and light chains are indicated and migrations of molecular mass standards in KDa are indicated at the left of the blots.

(C) In vitro pull-down assay showed that LAP1 binds to the nucleoplasmic domain of emerin. Immunoblot shows the input and GST-LAP1 and V5-tagged LAP1 purified from HEK 293 cells fused to agarose beads pulled down purified MBP-emerin fusion protein but not purified MBP. Analysis of bacterially expressed MBP-emerin showed intact protein (*) and smaller fragments (bracket). Migrations of molecular mass standards in KDa are indicated at the left of the blots.

(D) Schematic diagram of full-length human LAP1 (LAP1-FL), the nucleoplasmic domain plus transmembrane segment (LAP1-Nuc) and luminal domain plus transmembrane segment (LAP1-Lum) expressed in HEK 293 cells for the co-immunoprecipitation experiments shown in panel E. Red indicated V5 epitope and blue the transmembrane segment; amino acid residues 1, 330, 360 and 584 are indicated. The blue mesh indicates the relative position of the nuclear lamins and green rectangles the inner (INM) and outer (ONM) nuclear membranes [not to scale].

(E) Full-length LAP1 and the nucleoplasmic domain plus transmembrane segment bind emerin but the luminal domain plus the transmembrane segment does not. HEK 293 cells were transfected with vector only or plasmids expressing V5 tagged fusions of LAP1 as indicated. Protein extracts were collected and immunoprecipitated (IP) with anti-V5 antibodies. Protein inputs (1% of total lysate) and precipitated products were separated by SDS-PAGE, transferred to nitrocellulose and probed with antibodies against V5 or emerin as indicated. Migrations of molecular mass standards in KDa are indicated at the left of the blots.

See also Table S1.

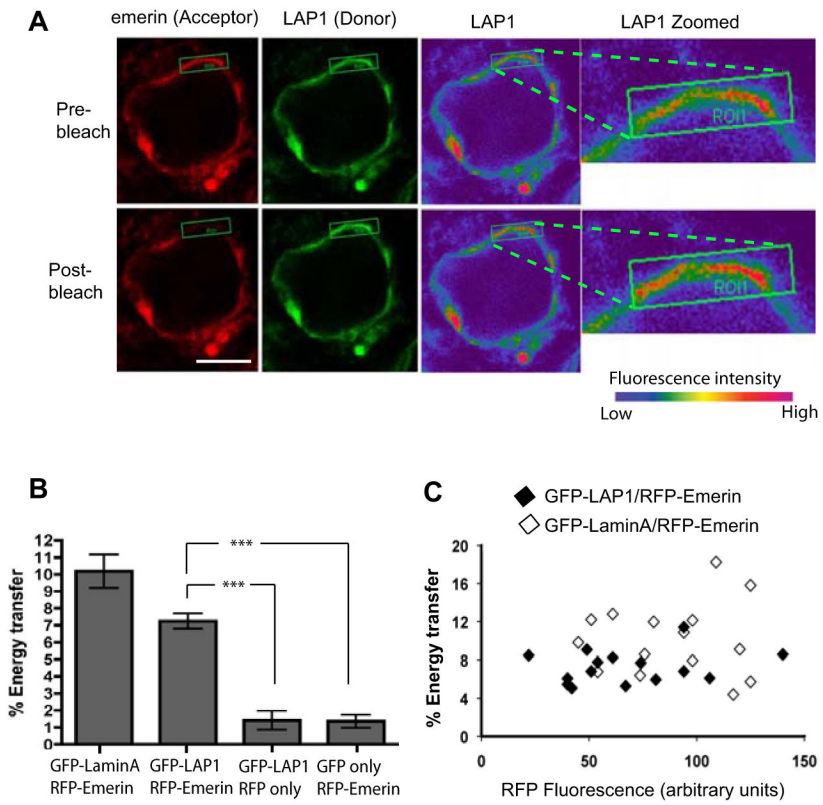


**Figure 2. FRET Analysis of LAP1 and Emerin Association in Cells**

(A) Representative images of a cell expressing RFP-emerin (Acceptor) and GFP-LAP1 (Donor). Images were taken pre (upper panel) and post (lower panel) photobleach of RFP-emerin in the boxed region of interest (ROI). In the two right panels (LAP1 and LAP1 Zoomed), intensities of GFP-LAP1 signals were mapped as colors in a rainbow spectrum from low and high fluorescence intensity as indicated; red signals demonstrate increased GFP-LAP1 fluorescence and show increased fluorescent intensity after a photobleaching. Bar: 5 μm.

(B) Calculated FRET energy transfers between the protein pairs indicated. Values are means ± SEMs; n = 15, ***$P$<0.001.

(C) Acceptor (RFP) fluorescence intensities prior to photobleaching (x-axis) plotted against energy transfers (y-axis) for the protein pairs indicated. Linear regression analysis of the plotted data sets of the indicated protein pairs showed no correlation between fluorescence intensities and FRET % energy transfers, confirming that the binding of protein pairs was specific.

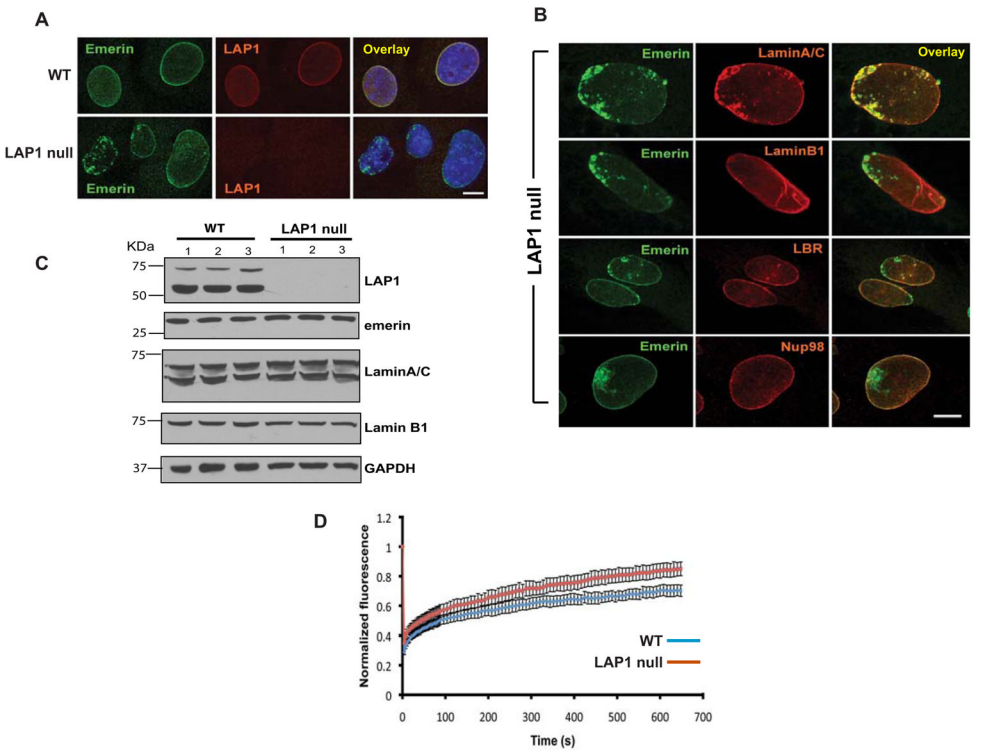


**Figure 3. Mislocalization of Emerin and Lamin A in LAP1 Null Fibroblasts**

(A) Confocal immunofluorescence micrographs showing emerin localization in fibroblasts from wild type (WT) and LAP1 null mice. Cells were labeled with antibodies against emerin (green) and LAP1 (red) with co-localization showing as yellow (Overlay); in overlays counterstaining of nuclei with DAPI (blue) is also shown. Bar: 10 μm.

(B) Confocal immunofluorescence micrographs showing the localization of emerin and other indicated proteins in LAP1 null fibroblasts. Cells were labeled with antibodies against emerin (green) and the other indicated protein (red) with co-localization showing as yellow (overlay). Bar: 10 μm.

(C) Proteins in extracts from fibroblasts of 3 different LAP1 null and control mice were collected and subjected to immunoblot analysis using antibodies against LAP1, emerin, lamin A/C, lamin B1 and GADPH. Migrations of molecular mass standards in KDa are indicated at the left of the blots.

(D) FRAP analysis of GFP-emerin in transfected wild type and LAP1 null mouse fibroblasts. Curve shows normalized fluorescence versus time after photobleaching an area of the nuclear envelope. Data at each measured time point are means ± SD (n = 20 for control cells; n = 22 for LAP1 null cells).

See also Figure S1.

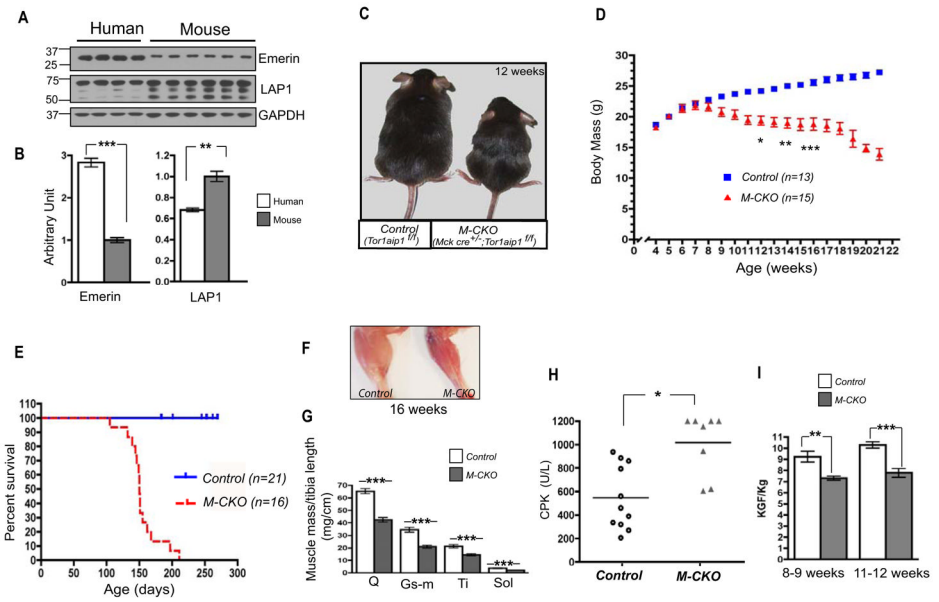


**Figure 4. Striated Muscle-selective Deletion of LAP1 in Mice Produces Shortened Lifespan with Progressive Muscle and Body Mass Loss**

(A) Immunoblots of protein extracts of lateral quadriceps muscle from normal adult humans and 6-week old wild type C57/B6 mice. Blots were probed with antibodies against emerin, LAP1 and GAPDH. Each lane is a sample from a different subject.

(B) Quantification of emerin and LAP1 expression normalized to GAPDH in protein extracts of mouse (n = 6) and human (n = 4) muscle samples. Values are means ± SEM; ***$P < 0.0001$, **$P < 0.005$.

(C) Photos of a littermate control (*Tor1aip1*$^{f/f}$) and an *M-CKO* (*Mckcre*$^{+/-}$;*Tor1aip1*$^{f/f}$) mouse at 12 weeks of age.

(D) Body mass of male *M-CKO* and control (*Tor1aip1*$^{f/f}$) mice versus age. Values are means ± SEM; *$P < 0.05$, **$P < 0.005$, ***$P < 0.0005$.

(E) Kaplan-Meier survival curves for male *Tor1aip1*$^{f/f}$ control and male *M-CKO* mice.

(F) Photos of skinned hindlimbs from a littermate control (*Tor1aip1*$^{f/f}$) and an *M-CKO* mouse at 16 weeks of age showing decreased muscle in the M-CKO mouse.

(G) Muscle mass to tibia length ratio of quadriceps (Q), gastrocnemius medialis (Gs-m), tibialis anterior (Ti) and soleus (Sol) muscles of *Tor1aip1*$^{f/f}$ control (n = 5) and *M-CKO* (n = 7) mice at 16 weeks of age. Values are means ± SEM; ***$P < 0.0005$.

(H) Serum creatine phosphokinase (CPK) activities in *Tor1aip1*$^{f/f}$ control (n=11) and *M-CKO* (n=8) mice at 8–9 weeks of age. The upper limit cut-off of the assay is 1,200 U/L. Values for each individual control (circles) and *M-CKO* (triangles) mouse are given and the horizontal bars are the mean values; *$P < 0.05$.

(I) Grip strength (kg force per kg) in *Tor1aip1*$^{f/f}$ control (n = 8) and *M-CKO* (n = 6) mice at 8–9 and 11–12 weeks of age. Values are means ± SEM; **$P < 0.005$, ***$P < 0.0005$.

See also Figure S2.

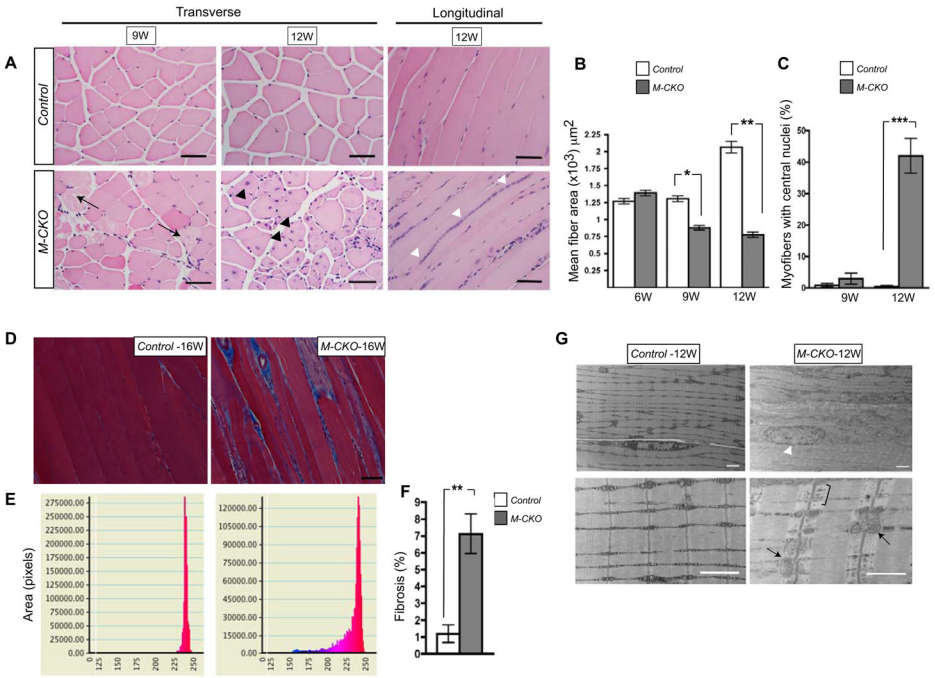


**Figure 5. Histopathological Analysis of Skeletal Muscle from *M-CKO* Mice**

(A) Representative hematoxylin and eosin-stained cross and longitudinal sections of quadriceps muscle from *Tor1aip1*$^{f/f}$ control and *M-CKO* mice at 9 (9W) and 12(12W) weeks of age (3 mice were analyzed per each group). Black arrows indicate degenerative/necrotic fibers, black arrowheads indicate central nuclei and white arrowheads indicate myonuclei arrays. Bars: 50 μm.

(B) Mean ± SEM of cross sectional fiber areas in quadriceps from *Tor1aip1*$^{f/f}$ control and *M-CKO* mice at 6 (6W), 9 (9W) and 12 (12W) weeks of age. Three different regions of each section from three different animals per group (n = 9) were analyzed. Values are means ± SEM; **P*< 0.01; ***P*< 0.001.

(C) Quantification of central nuclei in sections of quadriceps from *Tor1aip1*$^{f/f}$ control and *M-CKO* mice at 9 (9W) and 12 (12W) weeks of age. Three different regions from each section were counted (3 sections per animal; 3 animals per each age group). Note that about 40% of myofibers have central nuclei in quadriceps of 12-week old *M-CKO* mice. Values are means ± SEM; ****P*< 0.0001.

(D) Representative micrographs of sections of quadriceps muscle stained with Masson's trichrome from *Tor1aip1*$^{f/f}$ control mice (*Control-16W*) and *M-CKO* mice (*M-CKO-16*W) at 16 weeks of age. Areas of fibrosis stain blue; Bar: 50 μm.

(E) Hue histograms of micrographs in Panel D in which colors are represented from 0–255 units (blue 140–200 units) versus area of tissue section. Y-axis gives area (pixels) and X-axis the color spectrum with red color for muscle tissue and blue color (140–200 units) for connective tissue.

(F) Percentage of fibrosis per surface area of muscle. Sections of quadriceps from 16 week-old *Tor1aip1*$^{f/f}$ mice (*Control-16W*) and *M-CKO* mice were stained with Masson's trichrome measured as described in previous panel. Three different regions from each section from three different animals per group (n = 9) were analyzed. Values are means ± SEM; **P < 0.005.

(G) Representative electron micrographs of sections of quadriceps muscle from *Tor1aip1*$^{f/f}$ control mice (*Control-12W*) and *M-CKO* mice (*M-CKO-12W*) at 12 weeks of age. Bars: 2 μm. White arrowhead indicates an enlarged nucleus, black bracket indicates dispersed

glycogen particles and black arrows indicate enlarged mitochondria in muscle sections from a *M-CKO* mouse.
See also Figure S3.

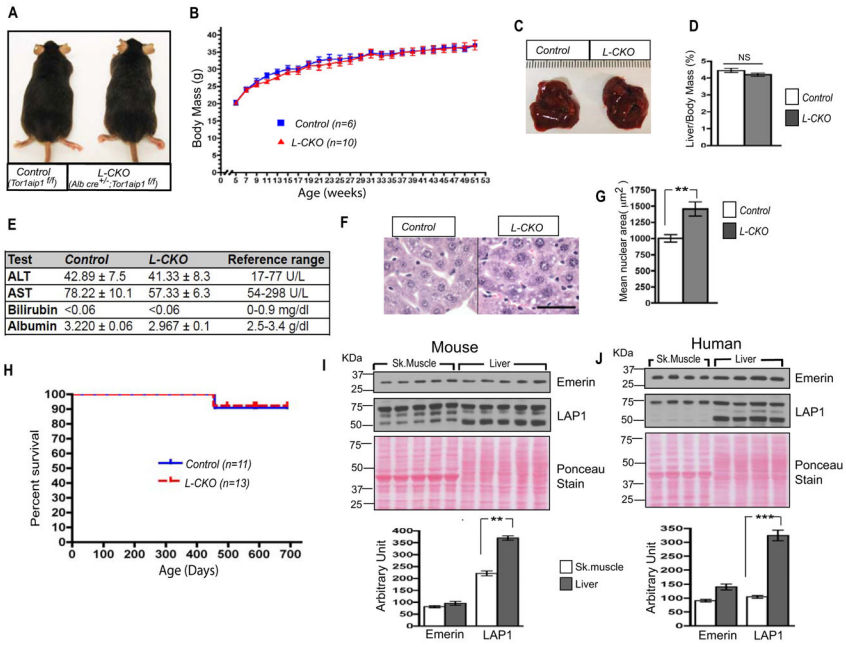


**Figure 6. Analysis of Mice with Liver-selective Deletion of LAP1**

(A) Photos of a littermate control (*Tor1aip1*$^{f/f}$) and *L-CKO* (*Albcre*$^{+/-}$;*Tor1aip1*$^{f/f}$) mouse at 16 weeks of age.

(B) Body mass of male *L-CKO* and control (*Tor1aip1*$^{f/f}$) mice versus age. Values are means ± SEM; differences between genotypes were not significant.

(C) Photos of livers from a littermate control (*Tor1aip1*$^{f/f}$) and an *L-CKO* mouse at 16 weeks of age.

(D) Liver to body mass ratio of *Tor1aip1*$^{f/f}$ control (n = 6) and *L-CKO* (n = 10) mice at 16 weeks of age. Values are means ± SEM; NS = not statistically significant.

(E) Serum aspartate aminotransferase (AST) and alanine aminotransferase (ALT) activities and albumin and bilirubin concentrations in *Tor1aip1*$^{f/f}$ control littermates (n = 9) and *L-CKO* (n = 9) mice at 16 weeks of age and normal reference ranges for these parameters in the Comparative Pathology Laboratory at Columbia University Medical Center. Values are means ± SEM.

(F) Representative hematoxylin and eosin-stained sections of liver from *Tor1aip1*$^{f/f}$ control mice and *L-CKO* mice at 16 weeks of age; Bar: 50 μm.

(G) Bar graph shows mean ± SEM of nuclear area per hepatocyte for *Tor1aip1*$^{f/f}$ control mice and *L-CKO* mice at 16 weeks of age; n = 100, $^{**}P < 0.005$.

(H) Kaplan-Meier survival curves for male *Tor1aip1*$^{f/f}$ control and male *L-CKO* mice. Mice were monitored up to 690 days of age; one mouse per each group died at ages greater than 400 days.

(I) Immunoblots of protein extracts of skeletal muscle (Sk. Muscle) and liver from 6-week old wild type C57/B6 mice. Blots were probed with antibodies against emerin and LAP1. Ponceau S-stained nitrocellulose sheet shows similar amounts of protein loading (20 μg of protein/lane) for each sample. Migrations of molecular mass standards in KDa are indicated at the left. Signal intensity was measured and averaged for emerin and LAP1 bands (bottom panel). Values are means ± SEM. ** $P < 0.005$.

(J) Immunoblots of protein extracts of human skeletal muscle (Sk. Muscle) and liver. Blots were probed with antibodies against emerin and LAP1. Ponceau S-stained nitrocellulose sheet shows similar amounts of protein loading (20 μg of protein/ lane) for each sample. Migrations of molecular mass standards in KDa are indicated at the left. Signal intensity was

measured and averaged for emerin and LAP1 bands (bottom panel). Values are means ± SEM. *** $P < 0.0001$.
See also Figure S4.

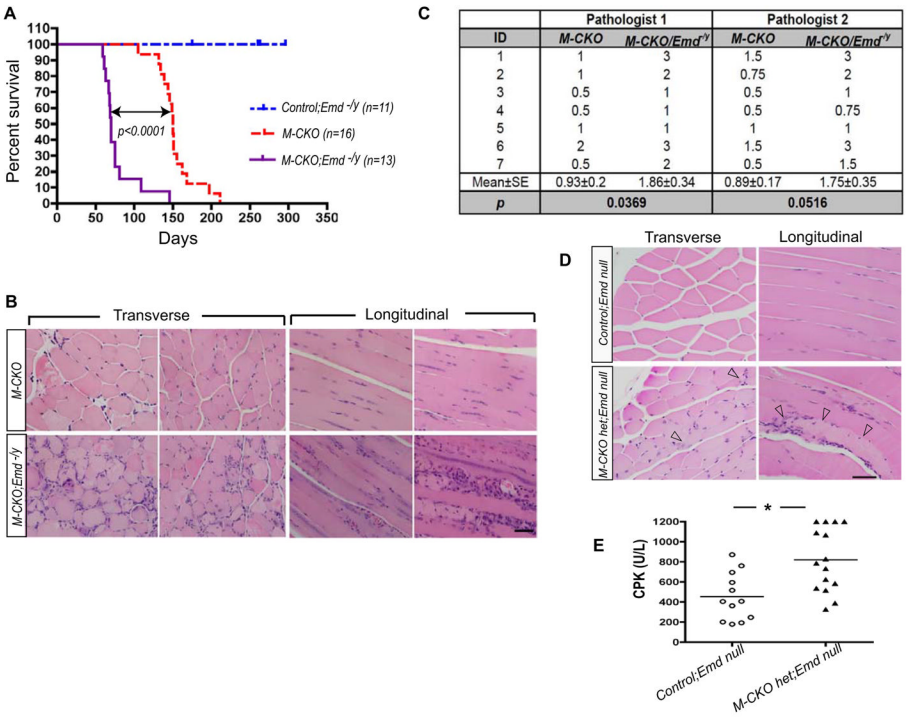


| | Pathologist 1 | | Pathologist 2 | |
|---|---|---|---|---|
| ID | M-CKO | M-CKO/Emd-/y | M-CKO | M-CKO/Emd-/y |
| 1 | 1 | 3 | 1.5 | 3 |
| 2 | 1 | 2 | 0.75 | 2 |
| 3 | 0.5 | 1 | 0.5 | 1 |
| 4 | 0.5 | 1 | 0.5 | 0.75 |
| 5 | 1 | 1 | 1 | 1 |
| 6 | 2 | 3 | 1.5 | 3 |
| 7 | 0.5 | 2 | 0.5 | 1.5 |
| Mean±SE | 0.93±0.2 | 1.86±0.34 | 0.89±0.17 | 1.75±0.35 |
| p | 0.0369 | | 0.0516 | |

**Figure 7. Shortened Lifespan and More Severe Myopathy in Mice with Combined Striated Muscle-selective LAP1 and Emerin Depletion**

(A) Kaplan-Meier survival curves for male *M-CKO*, *M-CKO;Emd*$^{-/y}$ and *Tor1aip1*$^{f/f}$*;Emd*$^{-/y}$ (*Control;Emd*$^{-/y}$) mice. Log-rank test was used to compare survival curves. The difference between *M-CKO* and *M-CKO;Emd*$^{-/y}$ mice was statistically significant ($P$<0.0001).

(B) Representative hematoxylin and eosin-stained transverse and longitudinal sections of quadriceps from male *M-CKO* and *M-CKO;Emd*$^{-/y}$ mice. Bar: 50 μm

(C) Myopathy severity scores of histopathological examinations for skeletal muscle from male *M-CKO* and *M-CKO;Emd*$^{-/y}$ mice. Individual scores for samples from 7 male *M-CKO* and 7 *M-CKO;Emd*$^{-/y}$ mice and mean ± SEM score given by two independent, blinded neuromuscular pathologists are shown. P-values for severity score differences between *M-CKO* and *M-CKO;Emd*$^{-/y}$ mice of each pathologist are shown.

(D) Hematoxylin and eosin-stained cross and longitudinal sections of quadriceps muscle from Control;Emd null (*Tor1aip1*$^{f/f}$*;Emd null*) and *M-CKO* het;Emd null (*Mck cre*$^{+/-}$*;Tor1aip1*$^{f/f}$*;Emd null*) mice at their 10 weeks of ages. Muscle sections from n=8 mice per each group were blindly examined by a pathologist. The sections from Control;Emd null group showed no pathology, while the sections from two out of eight *M-CKO* het;Emd null mice displayed occasional degenerative/necrotic fibers as indicated by arrowheads.

(E) Serum creatine phosphokinase (CPK) activities in Control;Emd null (n=12) and *M-CKO* het;Emd null mice (n=15) at their 8–11 weeks of ages. The upper limit cut-off of the assay is 1,200 U/L. Values for each individual Control;Emd null (circles) and *M-CKO* het;Emd null (triangles) mouse are given and the horizontal bars are the mean values; *$P$ <0.05.